

H-INFINITY CONTROL OF A 3-DOF RRR SPATIAL SERIAL MECHANISM

ISABELLA STEVANI*, ANDRÉ GARNIER COUTINHO†, DIEGO COLÓN*, TARCÍSIO ANTÔNIO HESS-COELHO†

**Departamento de Telecomunicações e Controle – PTC, Escola Politécnica da USP
Av. Prof. Luciano Gualberto, trav 3, 158, Cidade Universitária, São Paulo, BRAZIL*

†*Departamento de Engenharia Mecatrônica e de Sistemas Mecânicos – PMR, Escola Politécnica da USP*

Av. Prof. Mello Moraes, 2231, Cidade Universitária, São Paulo, BRAZIL

Emails: `isabella.stevani@usp.br`, `andre.garnier.coutinho@usp.br`, `diego@lac.usp.br`,
`tarchess@usp.br`

Abstract— The usage of serial manipulators in industry is very common, mostly for repetition tasks. Their dynamic models are nonlinear and usually involve uncertainties due to dynamic modeling error, dynamic parameter variation, unmodeled dynamics and unknown disturbances. To control this type of system, a combination of a feedback linearization algorithm and a H_∞ robust control method is proposed. Simulations have been performed to prove the control system robustness against model uncertainties.

Keywords— H-Infinity Control, Feedback Linearization, Serial Mechanism, Nonlinear Control, Robust Control.

Resumo— O uso de robôs seriais na indústria é muito comum, principalmente para tarefas repetitivas. Seus modelos dinâmicos são não-lineares e geralmente envolvem incertezas devido a erros de modelagem dinâmica, variação de parâmetros dinâmicos, dinâmicas não modeladas e distúrbios desconhecidos. Para controlar este tipo de sistema, uma combinação de linearização por realimentação e controle robusto H_∞ é proposta. Simulações foram realizadas para comprovar a robustez do sistema de controle frente à incertezas de modelo.

Palavras-chave— Controle H-Infinity, Linearização por Realimentação, Mecanismo Serial, Controle Não-linear, Controle Robusto.

1 Introduction

Serial manipulators are widely used in industry for material handling, pick and place operations and other processes that involve repeated movements (Moradi et al., 2010). Although serial mechanisms have simpler and more consolidated models than parallel ones, it is known that its dynamics are highly coupled and nonlinear, requiring a nonlinear controller or a robust linear controller capable of dealing with these nonlinearities.

Regarding the robust linear controller, the H_∞ control technique has been proved to be a powerful method to control not only nonlinear systems, but also systems with uncertainties due to dynamic modeling error, dynamic parameter variation, unmodeled dynamics and unknown disturbances (Franco et al., 2006; Fu and Mills, 2007; Lee and Cheng, 1996). Yet, the H_∞ control method assumes that the dynamic system is linear, so a linearization technique is needed to successfully apply it to a nonlinear system. One option is the feedback linearization procedure. Although its algorithm is complex to evaluate in real time applications, it has shown a good performance (Buondonno and De Luca, 2016).

In the work reported here, the proposed control system combines the performance of the feedback linearization algorithm with the robustness of the H_∞ control method to control a nonlinear uncertain system. The article is organized as follows. Section 2 describes the dynamic model of the 3-

DOF RRR spatial serial mechanism and Section 3 deduces the feedback linearization algorithm used to linearize it. Section 4 computes the H_∞ robust control and analyzes its robustness properties. Section 5 presents and discusses the simulation results. Finally, the conclusions are drawn in Section 6.

2 Dynamic Modeling

The dynamic model of a serial mechanism can be written as:

$$M(q)\ddot{q} + V(q, \dot{q}) + G(q) = \tau, \quad (1)$$

where $M(q)$ is the inertia matrix, $V(q, \dot{q})$ is the vector of centrifugal and Coriolis terms, $G(q)$ is the vector of gravitational forces, q is a column-matrix of independent generalized coordinates, whose entries are relative displacements of the joints, and τ is a column-matrix of the generalized actuators' efforts in the directions of the independent quasi-velocities \dot{q} (Coutinho and Coelho, 2016; Dobrianskyj et al., 2014; Craig, 2005).

To obtain the dynamic model of a 3-DOF RRR spatial serial mechanism (Fig. 1), the Lagrangian formalism was applied (Lanczos, 2012) using the Denavit-Hatemberg parameters described in Table 1. The resultant dynamic model is given by:

$$M(q) = \begin{bmatrix} D_{11} & D_{12} & D_{13} \\ D_{12} & D_{22} & D_{23} \\ D_{13} & D_{23} & D_{33} \end{bmatrix}, \quad (2)$$

$$V(q, \dot{q}) = \begin{bmatrix} D_{111} & D_{122} & D_{133} \\ D_{211} & D_{222} & D_{233} \\ D_{311} & D_{322} & D_{333} \end{bmatrix} \begin{bmatrix} \dot{q}_1^2 \\ \dot{q}_2^2 \\ \dot{q}_3^2 \end{bmatrix} + \quad (3)$$

$$2 \begin{bmatrix} D_{112} & D_{113} & D_{123} \\ D_{212} & D_{213} & D_{223} \\ D_{312} & D_{313} & D_{323} \end{bmatrix} \begin{bmatrix} \dot{q}_1 \dot{q}_2 \\ \dot{q}_1 \dot{q}_3 \\ \dot{q}_2 \dot{q}_3 \end{bmatrix}, \quad (4)$$

$$G(q) = [D_1 \quad D_2 \quad D_3]^T, \quad (4)$$

$$q = [q_1 \quad q_2 \quad q_3]^T, \quad (5)$$

$$\tau = [\tau_1 \quad \tau_2 \quad \tau_3]^T, \quad (6)$$

with its coefficients given in terms of the vector q , the mass m_i of the i^{th} rigid body of the mechanical system, l_i and l_{gi} whereas the first is the i^{th} link length and the second is the distance from the beginning of the i^{th} link to its center of mass, and the principal moments of inertia $J_{x_i}, J_{y_i}, J_{z_i}$ of the i^{th} mechanical system's rigid body in relation of its center of mass:

$$\begin{aligned} D_1 &= 0 \\ D_2 &= m_2 l_{g2} \cos(q_2) + m_3 (l_2 \cos(q_2) + l_{g3} \cos(q_2 + q_3)) \\ D_3 &= m_3 l_{g3} \cos(q_2 + q_3) \\ D_{11} &= J_{x_2} \sin^2(q_2) + J_{x_3} \sin^2(q_2 + q_3) + J_{y_1} + J_{y_3} \cos^2(q_2 + q_3) + (J_{y_2} + m_2 l_{g2}^2) \cos^2(q_2) + m_3 (l_2 \cos(q_2) + l_{g3} \cos(q_2 + q_3))^2 \\ D_{22} &= J_{z_2} + J_{z_3} + m_2 l_{g2}^2 + m_3 (l_2^2 + 2l_2 l_{g3} \cos(q_3) + l_{g3}^2) \\ D_{33} &= J_{z_3} + m_3 l_{g3}^2 \\ D_{12} &= D_{13} = 0 \\ D_{23} &= J_{z_3} + m_3 l_{g3} (l_2 \cos(q_3) + l_{g3}) \\ D_{111} &= D_{122} = D_{133} = 0 \\ D_{112} &= \frac{1}{2} \sin(2(q_2 + q_3)) (J_{x_3} - J_{y_3}) + \sin(2q_2) (J_{x_2} - J_{y_2} - m_2 l_{g2}^2) - 2m_3 (l_2 \cos(q_2) + l_{g3} \cos(q_2 + q_3)) (l_2 \sin(q_2) + l_{g3} \sin(q_2 + q_3)) \\ D_{113} &= \sin(q_2 + q_3) (-m_3 l_2 l_{g3} \cos(q_2) + (J_{x_3} - J_{y_3} - m_3 l_{g3}^2) \cos(q_2 + q_3)) \\ D_{123}, D_{222}, D_{212}, D_{213} &= 0 \\ D_{211} &= \frac{1}{2} (-J_{x_2} \sin(2q_2)) + (J_{y_2} + m_2 l_{g2}^2) \sin(2q_2) + m_3 (\sin(2q_2)) l_2^2 + 2l_2 l_{g3} \sin(2q_2 + q_3) + (-J_{x_3} + J_{y_3} + m_3 l_{g3}^2) \sin(2q_2) \\ D_{233} &= -m_3 l_2 l_{g3} \sin(q_3) \\ D_{311} &= (m_3 l_2 l_{g3} \cos(q_2) + (-J_{x_3} + J_{y_3} + m_3 l_{g3}^2) \cos(q_2 + q_3)) \sin(q_2 + q_3) \\ D_{322} &= m_3 l_2 l_{g3} \sin(q_3) \\ D_{333} &= 0 \\ D_{312} &= D_{313} = D_{323} = 0. \end{aligned} \quad (7)$$

Table 1: Denavit-Hatemberg parameters for the RRR spatial serial mechanism.

i	a_i	α_i	d_i	θ_i
1	0	$\pi/2$	l_1	θ_1
2	l_2	0	0	θ_2
3	l_3	0	0	θ_3

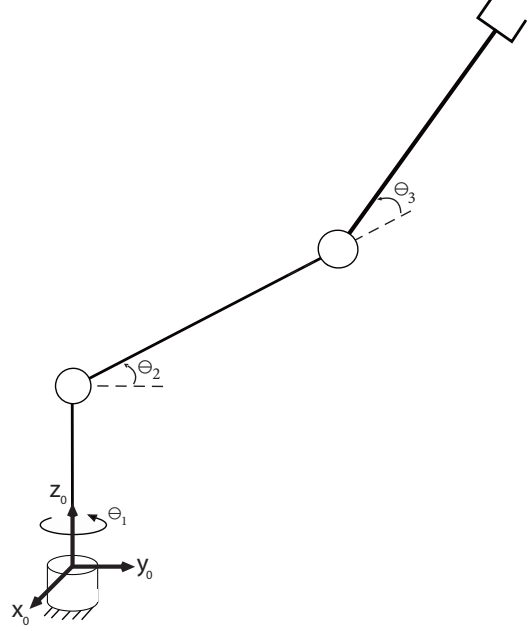


Figure 1: RRR spatial serial mechanism.

3 Feedback Linearization

The feedback linearization technique allows to obtain a linear input-output response from a nonlinear system by defining a new input to algebraically transform the original nonlinear system into a linear one (El Hajjaji and Ouladsine, 2001; Slotine et al., 1991; Craig, 2005). For the dynamic model presented in Section 2, the input τ could be defined in terms of a new input $\bar{\tau}$ as:

$$\tau = \alpha \bar{\tau} + \beta, \quad (8)$$

resulting in a new dynamic model given by:

$$M(q)\ddot{q} + V(q, \dot{q}) + G(q) = \alpha \bar{\tau} + \beta. \quad (9)$$

Defining $\alpha = M(q)$, $\beta = V(q, \dot{q}) + G(q)$ and $\bar{\tau} = -2\lambda\dot{q} - \lambda^2(q - \hat{\tau})$ with $\hat{\tau}$ as the new control signal and λ a scalar factor working as the natural frequency of $\bar{\tau}$, equation (9) becomes:

$$\ddot{q} + 2\lambda\dot{q} + \lambda^2 q = \lambda^2 \hat{\tau}, \quad (10)$$

which corresponds to the dynamic model of a second order linear system with transfer function ma-

trix given by:

$$\frac{q(s)}{\hat{\tau}(s)} = \frac{\lambda^2}{(s + \lambda)^2} \times I_3, \quad (11)$$

with I_3 as the third order identity matrix. However, in practice it's not possible to exactly remove all nonlinearities from (9) due to uncertain parameters in the system model. To design a controller capable of dealing not only with model uncertainties but also with external disturbances, a robust control technique is proposed in the next section.

4 H_∞ Control

The H_∞ control methods solve mathematical optimization problems to synthesize controllers that guarantee robust stability and performance of the closed-loop system. Despite the high level mathematical understanding needed to apply them successfully, H_∞ techniques have the advantage to be easily applicable to multi-variable systems with cross-coupling between channels.

Differently from classical control theory, the H_∞ control performance specifications are expressed not in terms of, for example, settling time or maximum peak response, but essentially in terms of the H_∞ norm. In the specific case of the H_∞ loop-shaping technique, performance specifications are defined through low and high frequency barriers (Skogestad and Postlethwaite, 2007). To fit the system response according to these barriers – thus guaranteeing robustness – pre and pos compensator functions must be defined to shape the controlled mechanism singular values into the desired format.

In order to synthesize a controller using H_∞ loop-shaping method and guarantee robustness, four steps need to be followed:

1. Define control requirements through frequency barriers;
2. Choose appropriate weight functions (W_1 and W_2) in order to impose that the shaped plant $G_s = W_2GW_1$ singular values respect the frequency barriers;
3. Solve the robust stabilization problem for the shaped plant $G_s = W_2GW_1$ to obtain the stabilizing controller K_s and then define H_∞ controller as $K = W_1K_sW_2$;
4. Verify robust stability and performance.

Since the feedback linearization algorithm turned the nonlinear system into a fully decoupled linear one given by (11), the system could be considered SISO during the H_∞ control design and the resulting controller could be expanded to the MIMO case at the end of the process.

4.1 Frequency barriers

Following the procedures described in (da Cruz, 1996), two barriers were defined: one at low frequency values to evaluate robust performance and one at high ones to evaluate robust stability.

The high frequency barrier regards model uncertainties. As done in (Stevens et al., 2015), assuming that the robot model is accurate to within 20% up to a frequency of $\omega = 200$ rad/s then growing without bound at the rate of 20 dB/decade after that, this behavior could be modeled by:

$$e_M(s) = \frac{s + 200}{1000}. \quad (12)$$

Thus, the robust stability barrier is approximately defined as:

$$RSB(s) = \frac{1}{e_M(s)} = \frac{1000}{s + 200}. \quad (13)$$

The low frequency barrier regards reference tracking and disturbance rejection. Supposing a maximum 10% reference tracking error up to $\omega = 80$ rad/s and a maximum 15% disturb rejection error up to $\omega = 100$ rad/s, the low frequency barrier that combines the most strict requirements coming from these two control objectives could be modeled by:

$$p(s) = \frac{1}{\alpha_p \frac{s}{\omega_p} + 1} = \frac{1000}{s + 100}, \quad (14)$$

with $\alpha_p = \min(0.1, 0.15)$ and $\omega_p = \max(80, 100)$, resulting in a robust performance barrier approximately defined as:

$$RPB(s) = \frac{p(s)}{1 - e_M(s)} = \frac{-1 \times 10^6}{(s - 800)(s + 100)}. \quad (15)$$

After all robustness barriers had been defined (Fig. 2), weight functions could be proposed.

As shown in Fig. 2, the robust performance barrier begins above the robust stability one, leading to an intersection between them. This means it's impossible to find a controller capable of fitting the closed-loop singular values under the robust stability barrier and the open-loop singular values above the robust performance barrier at the same time. In theoretical words, it's not possible to guarantee nominal performance for all plants considered within the model uncertainty, so the robust performance requirement could not be achieved by any controller.

4.2 Weight functions

Weight functions $W_1(s)$ and $W_2(s)$ work as pre and pos compensators for the nominal plant

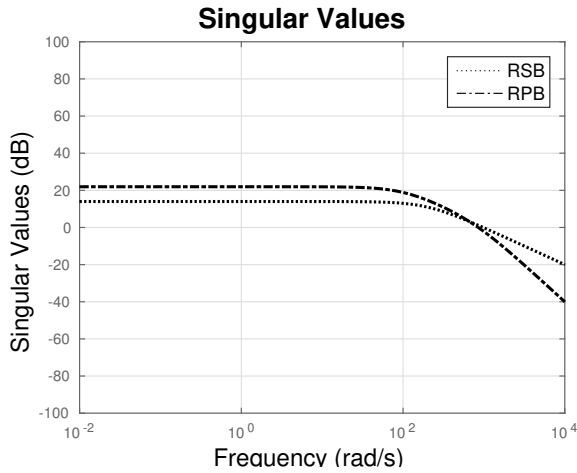


Figure 2: Robust stability (RSB) and performance (RPB) frequency barriers.

$G(s) = q(s)/\hat{\tau}(s)$ with $\lambda = 45$ rad/s. Intending to guarantee robust stability and performance, the weight functions should be chosen so that the shaped plant $G_s(s) = W_2GW_1$ respects robust performance barrier at low frequencies and robust stability barrier at high ones.

However, in this particular case, it's impossible to guarantee robust performance, so the weight functions were defined focusing in improving nominal performance and guaranteeing robust stability. To do so, Classical Control Theory guidelines regarding frequency domain designs were used to estimate the pre and pos compensators. Intending to increase the system's gain at low frequencies to minimize the stationary error without compromising the transient performance, a lag compensator was designed. Then, the gain was adjusted to respect the robust stability barrier, resulting in the weight functions given by:

$$W_1(s) = \frac{25(s + 11.5)}{(s + 0.19)}, \quad (16)$$

$$W_2(s) = 1. \quad (17)$$

The singular values of the resulting shaped plant $G_s(s)$ satisfy the robust stability condition as shown in Fig. 3.

4.3 Controller synthesis

Synthesize the H_∞ controller $K(s)$ means to solve a mathematical optimization problem. To do so, a simple option is to use the built-in function `ncfsyn` from the MATLAB Robust Control Toolbox[®] which provides the controller $K_s(s)$ used to compute the H_∞ controller $K(s) = W_2K_sW_1$ and the stability margin γ . The final second order MIMO controller $K(s) = \hat{\tau}(s)/r(s)$ where $r(s)$ regards

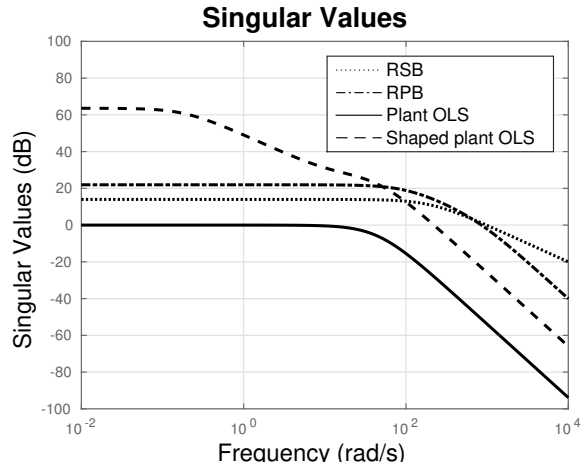


Figure 3: Robust stability (RSB) and performance (RPB) barriers and shaped plant open-loop system (OLS) response.

the reference signal is:

$$K(s) = \frac{47.40(s + 134.75)(s + 12.17)}{(s + 513.37)(s + 0.19)} \times I_3. \quad (18)$$

The nominal system's open loop model with the combination of the feedback linearization algorithm with the H_∞ controller results in:

$$\frac{q(s)}{r(s)} = K(s) \frac{\lambda^2}{(s + \lambda)^2}. \quad (19)$$

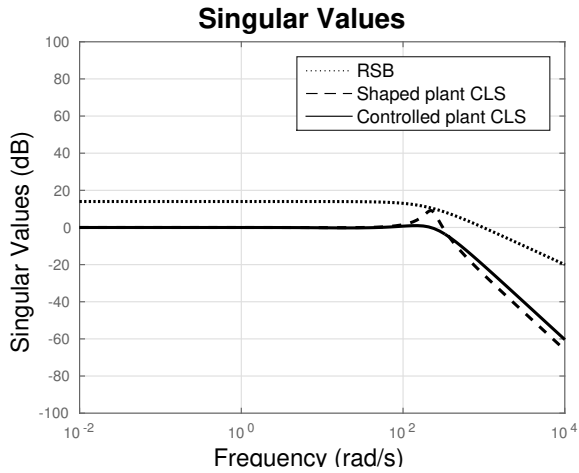
4.4 Robustness analysis

Verifying robust stability means to check if the closed-loop system's singular values are below the robust stability barrier, whereas assessing robust performance means to see if the open-loop system's singular values are above the robust performance barrier (da Cruz, 1996). According to Fig. 4, just the robust stability criteria is satisfied due to the impossibility of satisfaction of the robust performance criteria, concluding that the controller $K(s)$ can only guarantee robust stability.

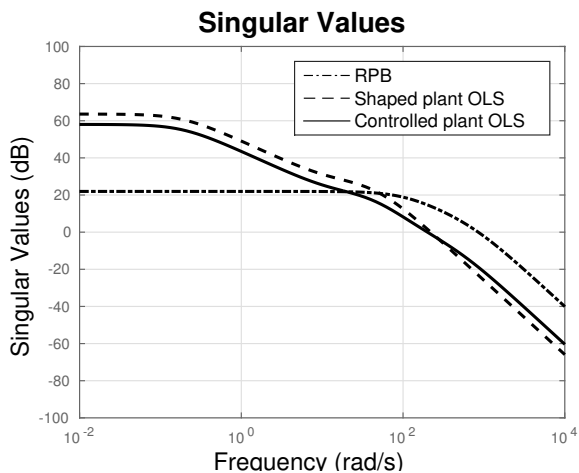
Also, as discussed in (Skogestad and Postlethwaite, 2007), given an H_∞ controller $K(s)$ with stability margin γ , the open-loop system KW_2GW_1 converges to the shaped plant W_2GW_1 if and only if $\epsilon = 1/\gamma \geq 0.2$. The controller described in (18) resulted in a stability margin $\gamma = 2.1436$, thus $\epsilon = 0.4665 \geq 0.2$ which satisfies the convergence condition as can be seen in Fig. 4.

5 Results and Discussion

To support the theoretical results presented in Subsection 4.4, simulations with sinusoidal inputs



(a) Robust stability barrier (RSB) and shaped and controlled plants closed-loop system (CLS) response.



(b) Robust performance barrier (RPB) and shaped and controlled plants open-loop system (OLS) response.

Figure 4: Robustness analysis.

were performed in the MATLAB/Simulink environment. The model parameters are shown in Table 2. For the gravity, the standard value $g = 9.8 \text{ m/s}^2$ was adopted.

A feedback linearization (FL) control with $\lambda = 100 \text{ rad/s}$ was also implemented for performance comparison. Its control law is defined by $\bar{\tau} = -2\lambda\dot{q} - \lambda^2(q - r)$ and follows (8), so that the nominal system open loop model considering only the feedback linearization control is given by:

$$\frac{q(s)}{r(s)} = \frac{\lambda^2}{(s + \lambda)^2}. \quad (20)$$

Feed forward terms were added in both control laws.

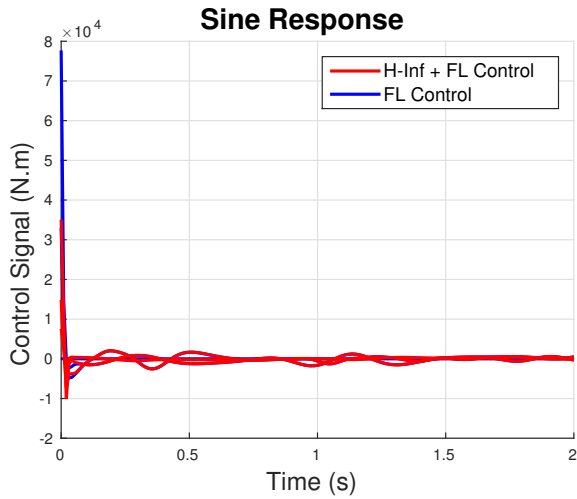
The first simulation considered the robot nominal parameters – that is, the exact values presented in Table 2 – and the results are shown in Fig. 5. Figs. 5(a) and 5(b) show that the H_∞ /feedback linearization combination and the FL technique only led almost to exact the same

Table 2: Robot nominal parameters.

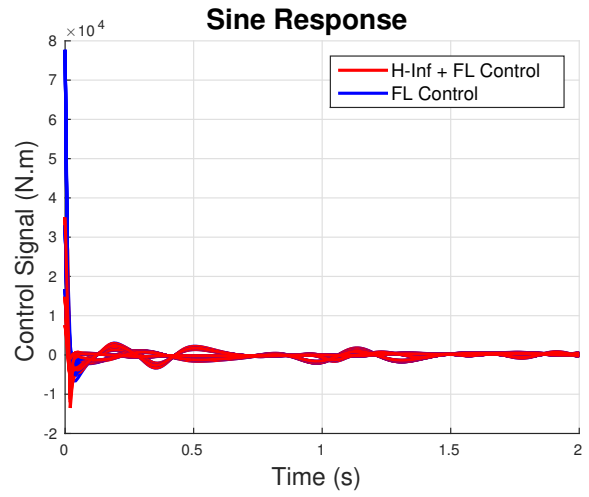
Parameter	Value
m_1	20 [kg]
m_2	20 [kg]
m_3	5 [kg]
l_1	1 [m]
l_2	1 [m]
l_3	1 [m]
l_{g1}	0.75 [m]
l_{g2}	0.75 [m]
l_{g3}	0.5 [m]
J_{x1}	1.6667 [kg.m ²]
J_{y1}	1.6667 [kg.m ²]
J_{z1}	0 [kg.m ²]
J_{x2}	0 [kg.m ²]
J_{y2}	1.6667 [kg.m ²]
J_{z2}	1.6667 [kg.m ²]
J_{x3}	0 [kg.m ²]
J_{y3}	0.4167 [kg.m ²]
J_{z3}	0.4167 [kg.m ²]

control signals with the exception of one component that the FL technique presented smaller values. In Fig. 5(c), the errors for a sinusoidal input are shown, concluding that the H_∞ /feedback linearization combination and the feedback linearization control provided equivalent results regarding the nominal model.

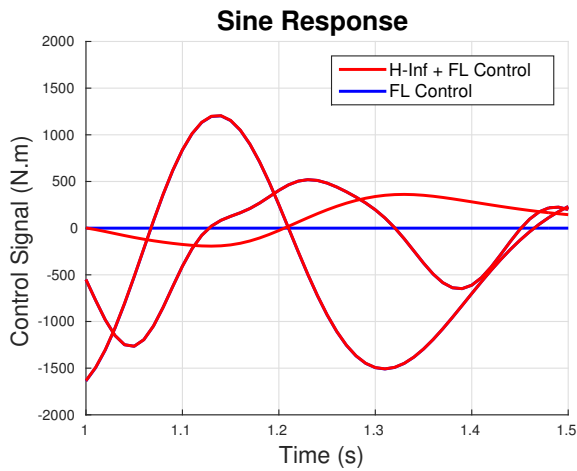
To perform the second simulation, 10 uncertain samples were considered for the robot model parameters from Table 2 within a 20% tolerance for the inertia parameters and a 5% tolerance for the link lengths, since the last ones could be precisely measured. The results are shown in Fig. 6. As in the nominal case simulation, in Figs. 6(a) and 6(b) the control signals of the H_∞ /feedback linearization combination and the FL technique only are very similar too, but now it was the H_∞ /feedback linearization combination that led to slightly smaller values. Fig. 6(c) show that, in the presence of remaining nonlinear dynamics, the H_∞ /feedback linearization combination led to almost a ten times better performance than only the feedback linearization control. This result was achieved due only to the H_∞ /feedback linearization combination robustness, since no significant increase in the control signal was observed – as a matter of fact, the H_∞ /feedback linearization combination control signals were slightly smaller than only the feedback linearization control ones.



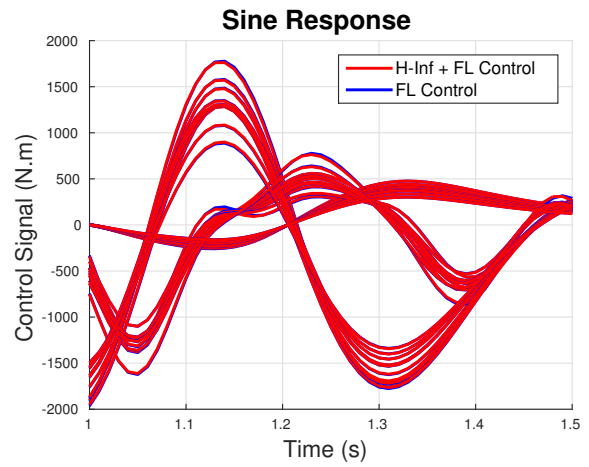
(a) Control signal.



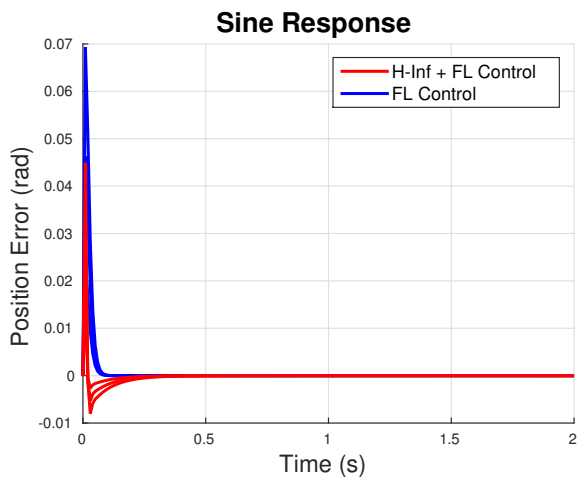
(a) Control signal.



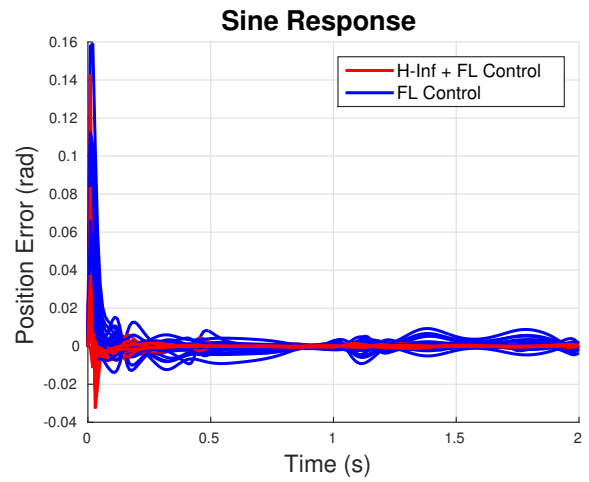
(b) Zoomed image of the control signal.



(b) Zoomed image of the control signal.



(c) Position error.



(c) Position error.

Figure 5: Nominal model response for sinusoidal input.

Figure 6: Uncertain model response for sinusoidal input.

6 Conclusions

The simulations have shown that the combination of a feedback linearization algorithm and a linear robust H_∞ controller is sufficiently robust to

control a nonlinear uncertain model, which in this case of study was a 3-DOF RRR spatial mechanism. More than that, it has shown that this combination leads to better performance using basically the same energy in comparison to use only

the feedback linearization control technique, regarding uncertain models. Future work will apply this control configuration on more complex structures, such as parallel mechanisms.

Acknowledgments

The authors would like to thank Coordenação de Aperfeiçoamento de Pessoal de Nível Superior (CAPES) for the first author's scholarship (process number 1771660) and Programa de Pós-Graduação em Engenharia Elétrica (PPGEE) from POLI – USP for the financial support to the first author participation in this conference. Also, the authors acknowledge the collaboration of Arthur Castello Branco de Oliveira.

References

- Buondonno, G. and De Luca, A. (2016). Efficient computation of inverse dynamics and feedback linearization for vsa-based robots, *IEEE Robotics and Automation Letters* **1**(2): 908–915.
- Coutinho, A. G. and Coelho, T. A. H. (2016). A new approach for obtaining the dynamic balancing conditions in serial mechanisms, *International Journal of Mechanisms and Robotic Systems* **3**(1): 32–47.
- Craig, J. J. (2005). *Introduction to robotics: mechanics and control*, Vol. 3, Pearson/Prentice Hall Upper Saddle River, NJ, USA:.
- da Cruz, J. J. (1996). *Controle Robusto Multivariável: O Método LGQ/LTR Vol. 05*, EdUSP.
- Dobrianskyj, G. M., Coutinho, A. G. and Hess-Coelho, T. A. (2014). Development of a controller for a 3-dof robotic platform for user interaction in rehabilitation therapies, *Biomedical Robotics and Biomechatronics (2014 5th IEEE RAS & EMBS International Conference on, IEEE*, pp. 819–824.
- El Hajjaji, A. and Ouladsine, M. (2001). Modeling and nonlinear control of magnetic levitation systems, *IEEE Transactions on Industrial Electronics* **48**(4): 831–838.
- Franco, A. L. D., Bourlès, H., De Pieri, E. R. and Guillard, H. (2006). Robust nonlinear control associating robust feedback linearization and h/sub/spl infin//control, *IEEE transactions on automatic control* **51**(7): 1200–1207.
- Fu, K. and Mills, J. K. (2007). Robust control design for a planar parallel robot, *International Journal of Robotics & Automation* **22**(2): 139.
- Lanczos, C. (2012). *The variational principles of mechanics*, Courier Corporation.
- Lee, G.-W. and Cheng, F.-T. (1996). Robust control of manipulators using the computed torque plus h-infinity compensation method, *IEE Proceedings-Control Theory and Applications* **143**(1): 64–72.
- Moradi, M., Nikoobin, A. and Azadi, S. (2010). Adaptive decoupling for open chain planar robots, *Scientia Iranica. Transaction B, Mechanical Engineering* **17**(5): 376.
- Skogestad, S. and Postlethwaite, I. (2007). *Multivariable feedback control: analysis and design*, Vol. 2, Wiley New York.
- Slotine, J.-J. E., Li, W. et al. (1991). *Applied nonlinear control*, Vol. 199, Prentice hall Englewood Cliffs, NJ.
- Stevens, B. L., Lewis, F. L. and Johnson, E. N. (2015). *Aircraft control and simulation: dynamics, controls design, and autonomous systems*, John Wiley & Sons.